Y.-W. Lin, S. Lee, S.-S. Li, Y. Xie, Z. Ren, and C. T.-C. Nguyen, "60-MHz wine glass micromechanical disk reference oscillator," Digest of Technical Papers, 2004 IEEE International Solid-State Circuits Conference, San Francisco, California, Feb. 15-19, 2004, pp. 322-323.

## 17.7 60-MHz Wine-Glass Micromechanical-Disk Reference Oscillator

Yu-Wei Lin, Seungbae Lee, Sheng-Shian Li, Yuan Xie, Zeying Ren, Clark T.-C. Nguyen

University of Michigan, Ann Arbor, MI

The quartz crystal used in the reference oscillator in a wireless communication transceiver is among the most difficult to integrate on chip. On-chip devices capable of matching its $Q$ (on the order of 10,000) and temperature stability (<35ppm over 0-70°C) are generally unavailable. Recently, an on-chip vibrating clamped-clamped beam (CC-beam) micromechanical resonator based on MEMS technology has been demonstrated at 10MHz with a $Q$ of 4,000 and a frequency stability of 34ppm [1] over 0-70°C, which matches that of quartz. Unfortunately, a recently demonstrated 10MHz oscillator using a wide-beam variant of this resonator [2] exhibits a far-from-carrier phase noise of only -120dBc/Hz—a value caused mainly by the insufficient power handling ability of the CC-beam micromechanical resonator device used [3].

This work achieves an effective 25dB improvement in phase noise performance over the previous 10MHz oscillator by replacing its wide-CC-beam resonator with a 60MHz, MEMS-based, wine glass disk micromechanical resonator [4] (c.f., Fig. 17.7.1), which has a 55X higher power handling capability, a comparable series motional resistance, and a 45X higher $Q$ of 48,000. The combination of this micromechanical resonator with a CMOS transresistance sustaining amplifier, implemented in the TSMC 0.35µm process and designed to accept the high impedance of the wine glass disk, yields a 60MHz reference oscillator that achieves a phase noise density of -100dBc/Hz at 1kHz offset from the carrier, and -130dBc/Hz at far-from-carrier offsets. Dividing down to 10MHz for fair comparison, these values correspond to -115dBc/Hz at 1kHz offset from a 10MHz carrier, and an effective -145dBc/Hz far-from-carrier value.

As shown in Fig. 17.7.1, the wine glass disk resonator of this work consists of a 3µm-thick disk supported by two beams that attach to the disk at its nodal points, which are motionless when the disk vibrates in its wine glass mode shape, shown in Fig. 17.7.2. In this mode shape, the disk expands along one axis and contracts along the orthogonal axis. To excite vibrations in this mode shape, a dc-bias voltage $V_P$ is applied to the disk structure, and an ac input signal $v_i$ to oppositely located input electrodes. These voltages result in a force proportional to the product $V_P v_i$ that drives the resonator into its vibration mode shape. This occurs when the frequency of $v_i$ matches the wine glass resonance frequency, given by

$$\left[\Psi_n\left(\frac{\zeta}{\xi}\right)-n-q\right]\left[\Psi_n(\zeta)-n-q\right]=(nq-n)^2 \quad (1)$$

where

$$q=\frac{\zeta^2}{2n^2-2}\,,\quad \zeta=2\pi f_o R\sqrt{\frac{\rho(2+2\sigma)}{E}}\,,\quad \xi=\sqrt{\frac{2}{1-\sigma}}\,,\quad n=2 \quad (2)$$

and where $\psi$ is a modified Bessel function quotient, $f_o$ is the resonant frequency, R is the disk radius, and ρ, σ, and E, are the density, Poisson ratio, and Young's modulus, respectively, of the disk structural material. Once vibrating, the dc-biased (by $V_P$) time-varying output electrode-to-resonator capacitors generate output currents given by $i_o = V_P$ (dC/dt). Seen through its terminals, the whole device can be equated to the LCR tank circuit shown in Fig. 17.7.1, for which the series motional resistance $R_x$ is

$$R_x=\frac{\sqrt{KM}\,d^4}{Q\varepsilon_o^2A^2V_p^2} \quad (3)$$

where K and M are the effective stiffness and mass of the disk, and d and A are the electrode-to-resonator gap and overlap area, respectively.

The key to achieving improvements on the present scale lies not only in the use of a wine glass disk resonator, but also in the specific advances applied to its design. In particular, the wine glass disk of this work differs from that of a previous prototype [4] in that its thickness is increased to 3µm and gap d reduced from 100nm to 80nm to increase its power handling and lower its impedance according to (3). The number of supports used is reduced from four to two, in order to decrease energy loss from the disk to the substrate through anchors, and thus, maximize the device $Q$. In addition, the stiffness of this wine glass disk is 6.6e5N/m, more than 55X the 1.2e4N/m of the 10MHz wide-CC-beam device, effectively allowing it to handle powers 55X higher. Even with these enhancements, using (3), the $R_x$ is 1.5kΩ for a 64µm-diameter 60MHz wine glass disk with $V_P$=12V and $Q$=48,000, larger than the 50Ω normally exhibited by a off-chip quartz crystals. Consequently, a sustaining amplifier capable of supporting high tank impedance is required.

To minimize $Q$ loading of the high impedance micromechanical resonator, a transresistance CMOS sustaining amplifier is used as shown in Fig. 17.7.3. The circuit of Fig. 17.7.3 differs from previous two-stage circuits [5] in that it achieves the needed 0° phase shift for oscillation with a single stage improving both its noise and bandwidth performance. As shown in the coarse oscillator schematic of Fig. 17.7.4, the sustaining circuit is composed of a fully balanced differential CMOS op amp connected in shunt-shunt feedback to one side. By taking the output from the other side of the differential op amp, an additional 180° phase shift is added to the 180° shift from the shunt-shunt feedback, resulting in a total 0° phase shift from input to output, while preserving the low output resistance (due to symmetry) obtained via shunt-shunt feedback. In the detailed circuit schematic of Fig. 17.7.3, transistors $M_1$-$M_5$ comprise the basic differential op amp, while $M_{11}$-$M_{18}$ constitute a common-mode feedback circuit that sets its bias point. The MOS resistor $M_{Rf}$ serves as a shunt-shunt feedback element that allows control of the transresistance gain via adjustment of its gate voltage. Figure 17.7.5 presents a photomicrograph of the amplifier IC. The chip area is about 50µm×50µm, which with the 105µm×105µm required for the wine glass disk, yields a tiny combined footprint of less than 160µm×160µm.

Wine glass disk resonators were fabricated via a three-polysilicon self-aligned stem process used previously to achieve disk resonators [4]. Figure 17.7.6 presents the SEM of a fabricated 60MHz wine glass disk, supported by only two support beams, that achieves a measured $Q$ of 48,000. Figure 17.7.7 presents the oscillator phase noise spectrum measured using an HP E5500 Phase Noise Measurement System, showing phase noise densities of -100dBc/Hz at 1kHz offset from the carrier, and -130dBc/Hz at far-from-carrier offsets. As previously mentioned the phase noise after frequency division from 60MHz to 10MHz is about 15dB better in each of the above categories. The spectrum of Fig. 17.7.7 differs from that generally seen for conventional reference oscillators in that it exhibits a $1/f^3$ noise dependence at close-to-carrier offsets where $1/f^2$ is normally expected. This $1/f^3$ dependence substantially degrades the close-to-carrier phase noise performance of this micromechanical resonator oscillator and is suspected to arise from hard limiting of this particular oscillator, which, in the future, may be alleviated by automatic level control [6].

*References:*

[1] W.-T. Hsu, J. R. Clark, and C. T.-C. Nguyen, "A Sub-Micron Capacitive Gap Process for Multiple-Metal-Electrode Lateral Micromechanical Resonators," *Technical Digest*, MEMS'01, pp. 349-352, Jan. 2001.

[2] Y.-W. Lin, S. Lee, Z. Ren, and C. T.-C. Nguyen, "Series-Resonant Micromechanical Resonator Oscillator," to be published in the *Technical Digest*, IEDM'03, Dec. 2003.

[3] T. Mattila, et al, "A 12 MHz Micromechanical Bulk Acoustic Mode Oscillator," *Sensors and Actuators A: Physical*, vol. 101, issues 1-2, pp. 1-9, Sep. 2002.

[4] M. A. Abdelmoneum, M. U. Demirci, and C. T.-C. Nguyen, "Stemless Wine-Glass-Mode Disk Micromechanical Resonators," *Technical Digest*, MEMS'03, pp. 698-701, Jan. 2003.

[5] C. T.-C. Nguyen and R. T. Howe, "An Integrated CMOS Micromechanical Resonator High-Q Oscillator," *IEEE J. Solid-State Circuits,* vol. 34, no. 4, pp. 440-455, April 1999.

[6] S. Lee and C. T.-C. Nguyen, "Influence of Automatic Level Control on Micromechanical Resonator Oscillator Phase Noise," *Proceedings of Frequency Control Symposium'03*, pp. 341-349, May 2003.

 

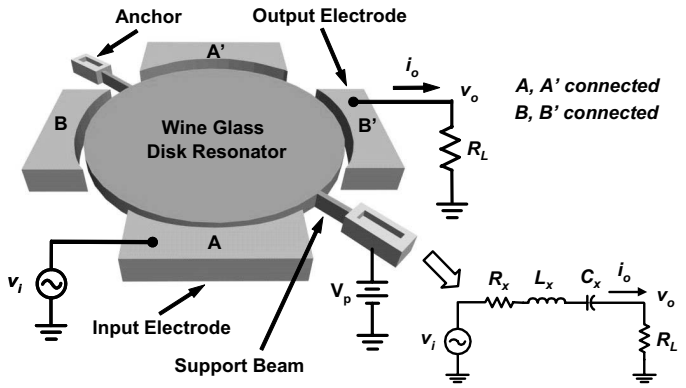


Figure 17.7.1: Perspective-view schematic of the micromechanical wine-glass-mode disk resonator in a typical two-port bias and excitation configuration with an equivalent LCR circuit model.

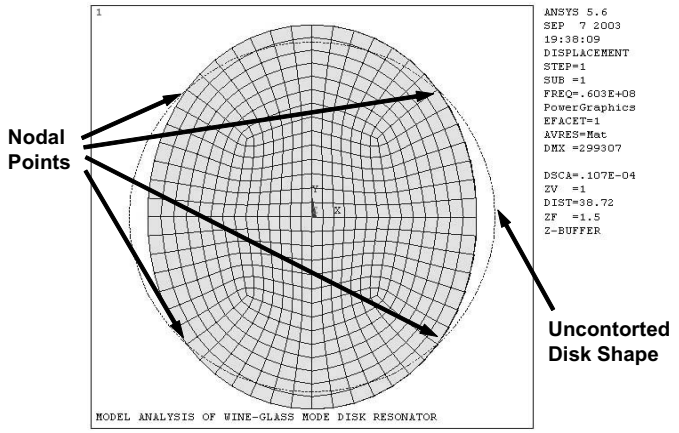


Figure 17.7.2: Mode shape for the wine-glass-mode disk resonator of Fig. 17.7.1 simulated via finite element analysis (ANSYS).

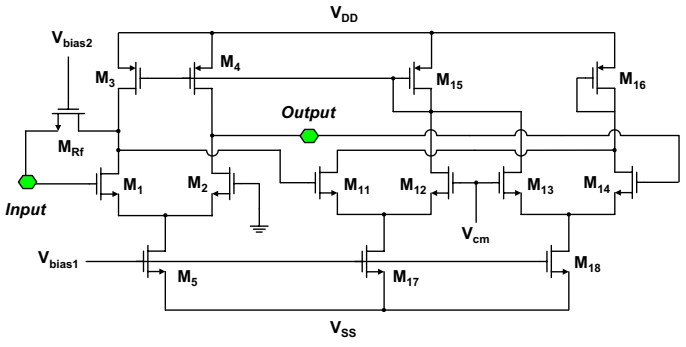


Figure 17.7.3: Detailed circuit schematic of the sustaining transresistance amplifier of this work, implemented by a fully-differential amplifier in a shunt-shunt feedback configuration.

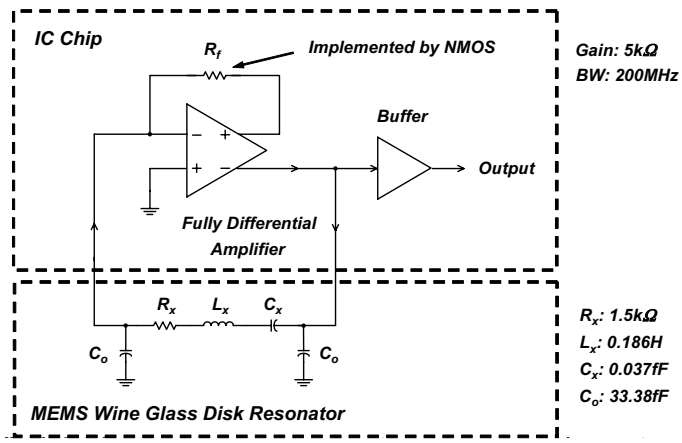


Figure 17.7.4: Top-level circuit schematic of the micromechanical resonator oscillator of this work. Here, the micromechanical resonator is represented by its equivalent electrical circuit.

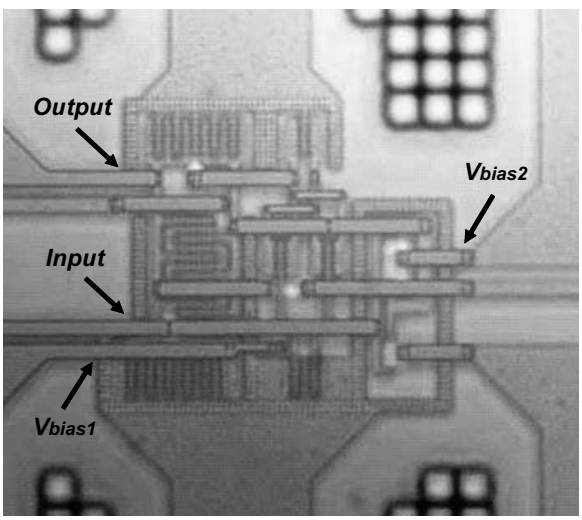


Figure 17.7.5: Photo of the sustaining transresistance amplifier fabricated in TSMC's 0.35μm CMOS process.

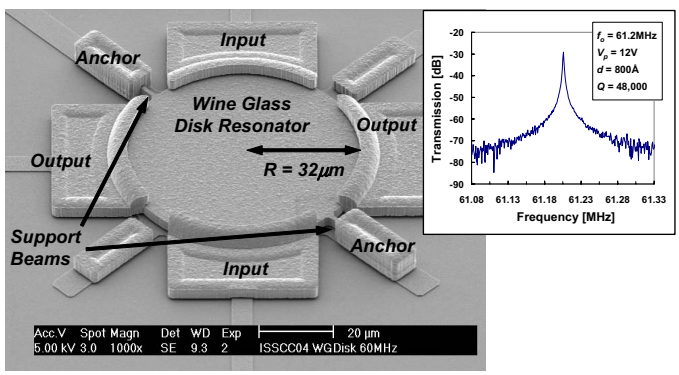


Figure 17.7.6: Scanning electron micrograph (SEM) of a fabricated wine glass disk resonator with two supports, with its measured frequency characteristic.


0-7803-8267-6/04 

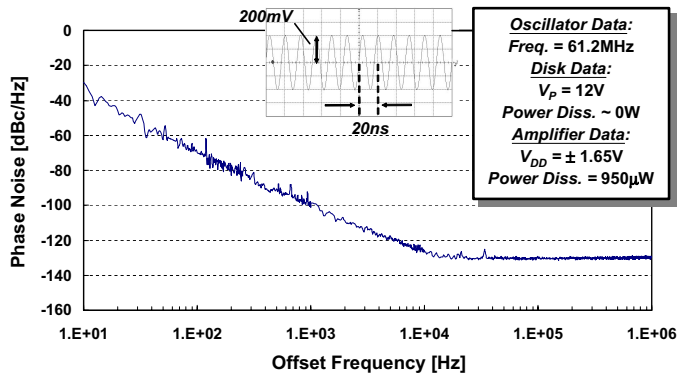


**Figure 17.7.7: Phase noise density versus carrier offset frequency plot for the micromechanical resonator oscillator of Figure 17.7.4, measured by an HP E5500 Phase Noise Measurement System.**

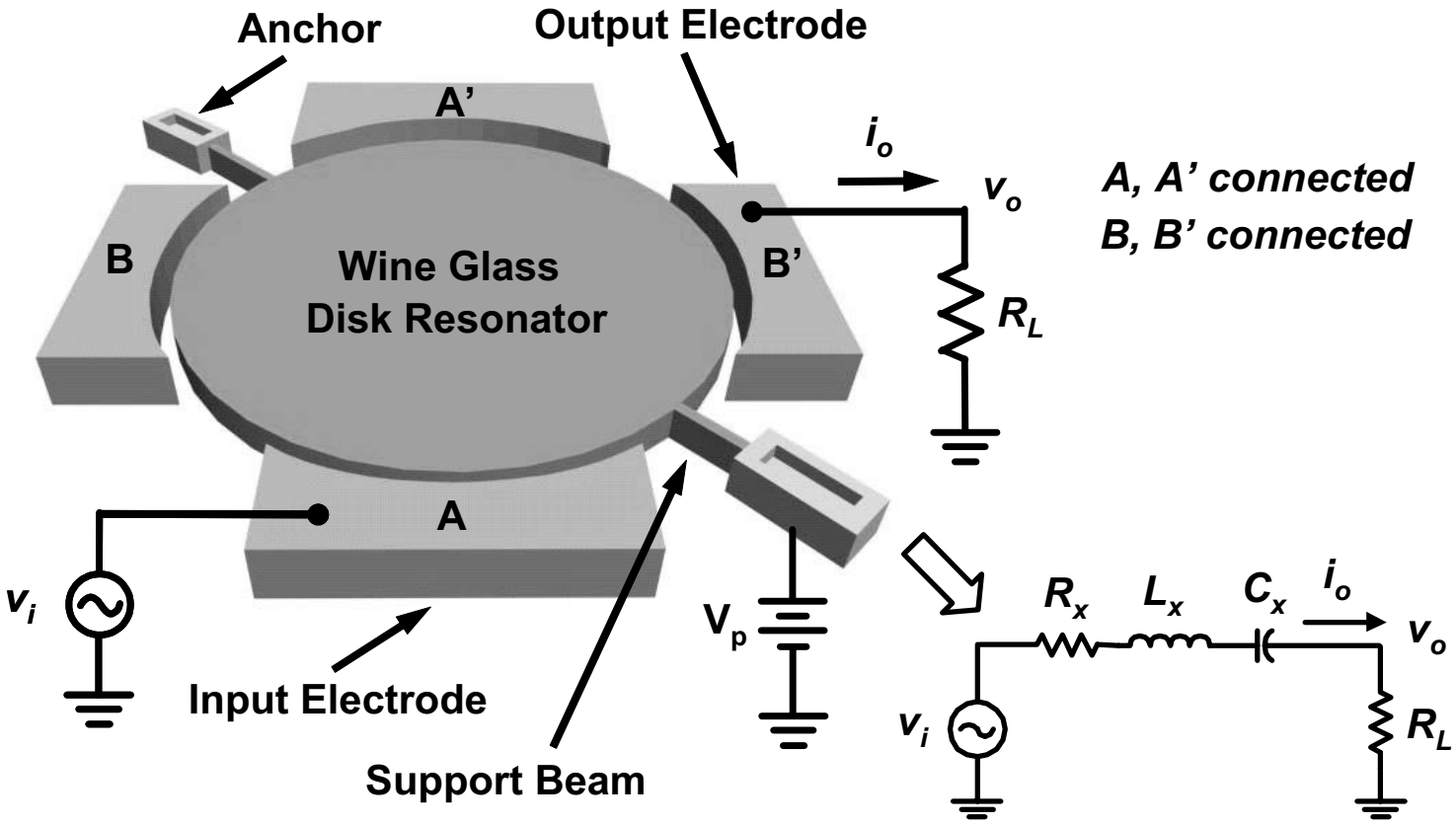


**Figure 17.7.1: Perspective-view schematic of the micromechanical wine-glass-mode disk resonator in a typical two-port bias and excitation configuration with an equivalent LCR circuit model.**


0-7803-8267-6/04 

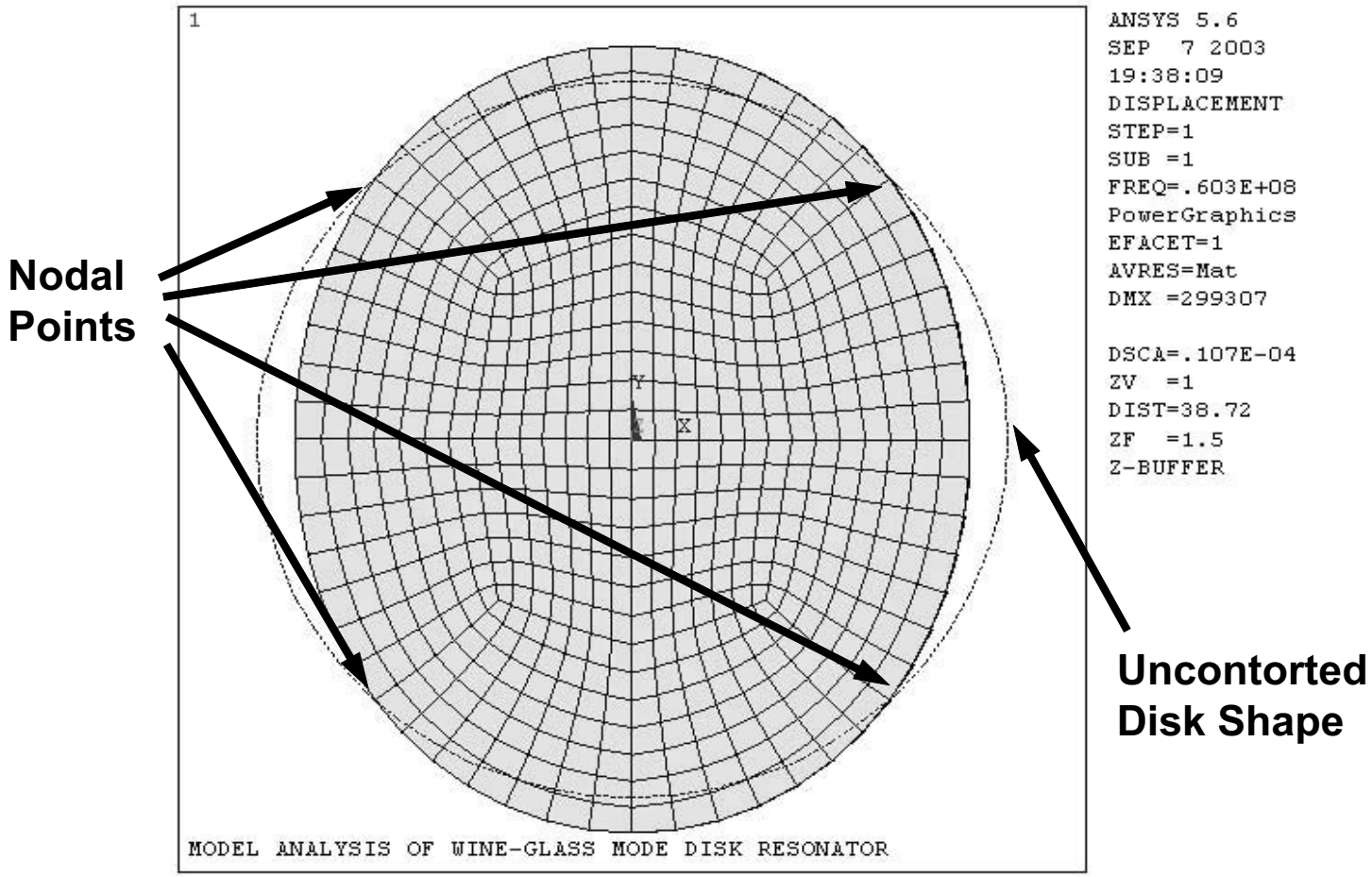


**Figure 17.7.2: Mode shape for the wine-glass-mode disk resonator of Fig. 17.7.1 simulated via finite element analysis (ANSYS).**

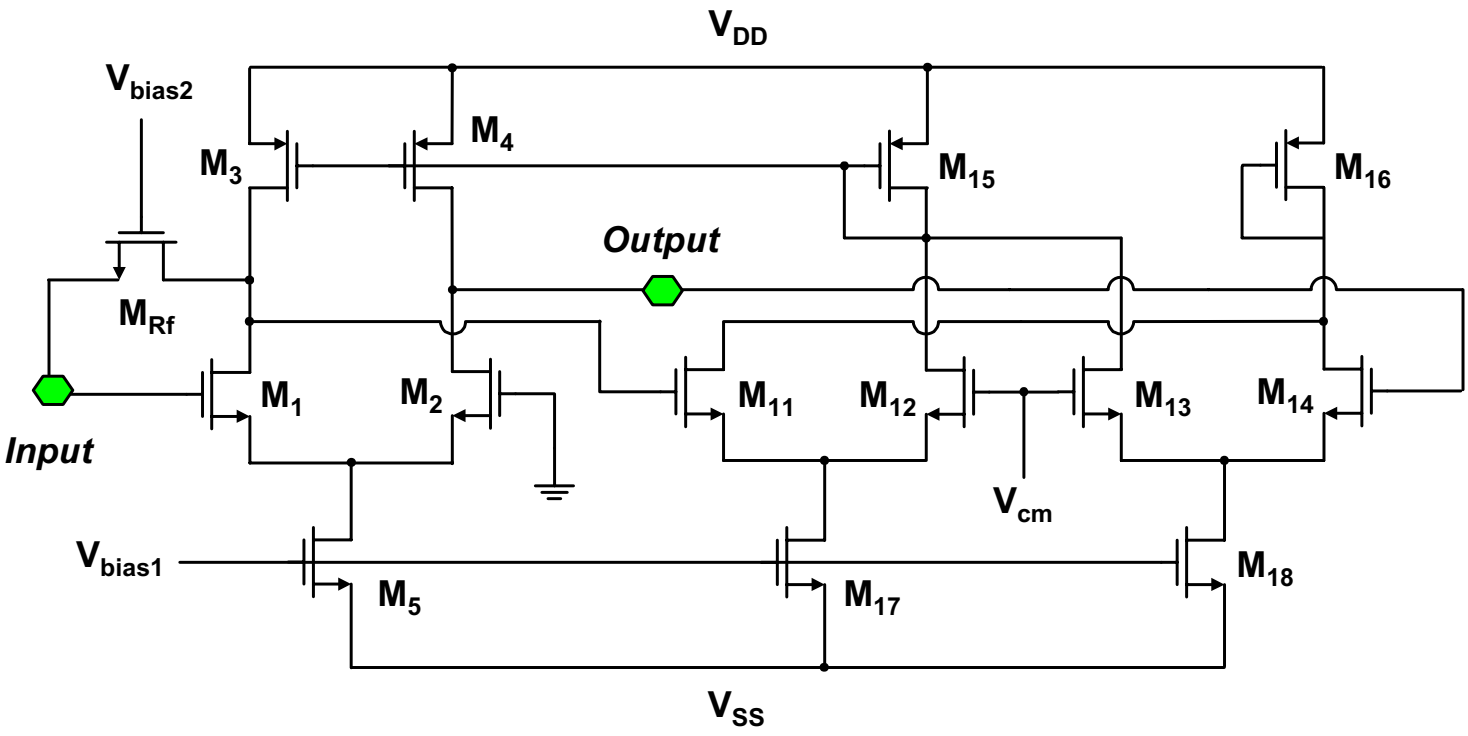


**Figure 17.7.3: Detailed circuit schematic of the sustaining transresistance amplifier of this work, implemented by a fully-differential amplifier in a shunt-shunt feedback configuration.**


0-7803-8267-6/04 

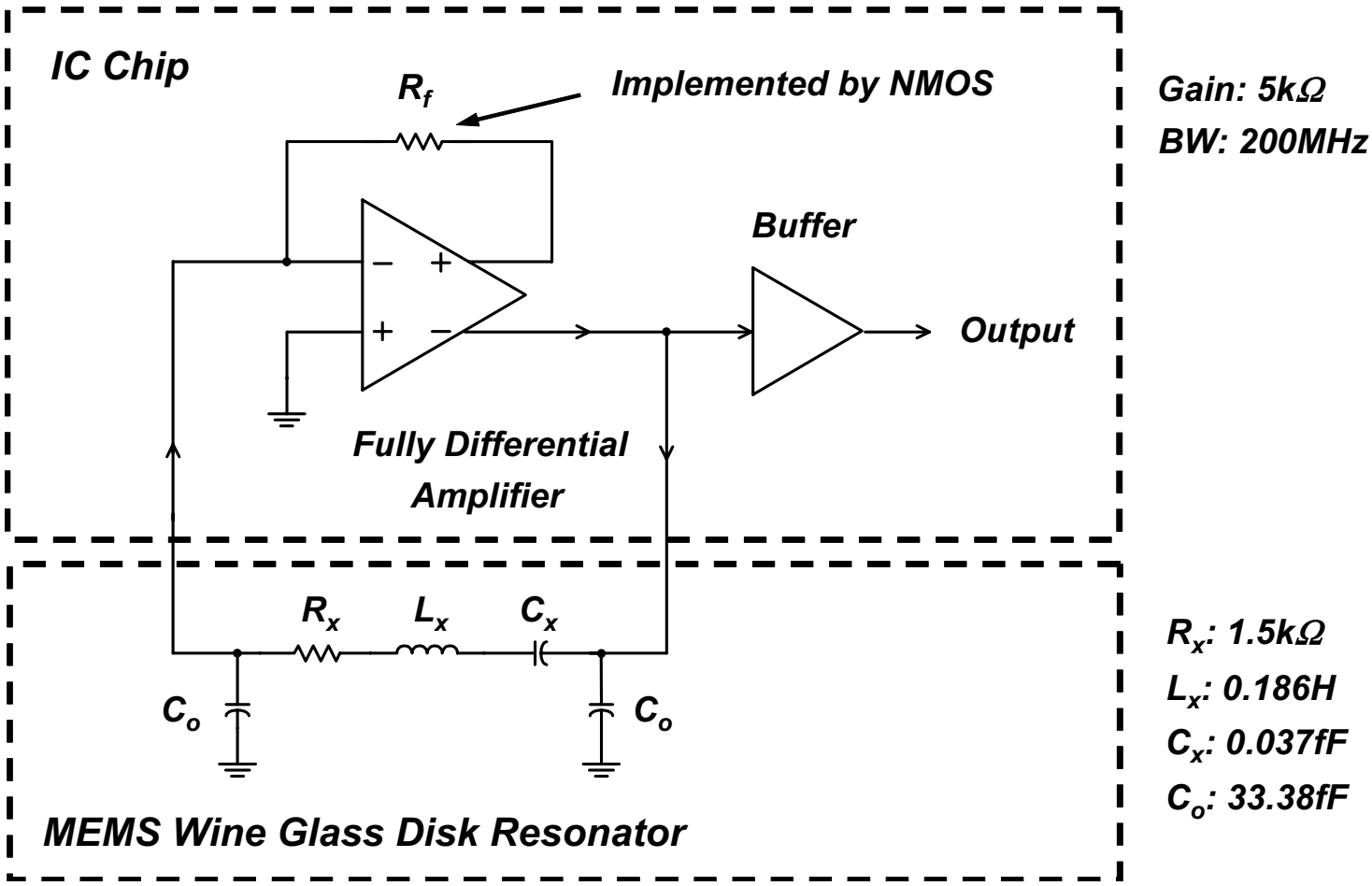


**Figure 17.7.4: Top-level circuit schematic of the micromechanical resonator oscillator of this work. Here, the micromechanical resonator is represented by its equivalent electrical circuit.**


0-7803-8267-6/04 

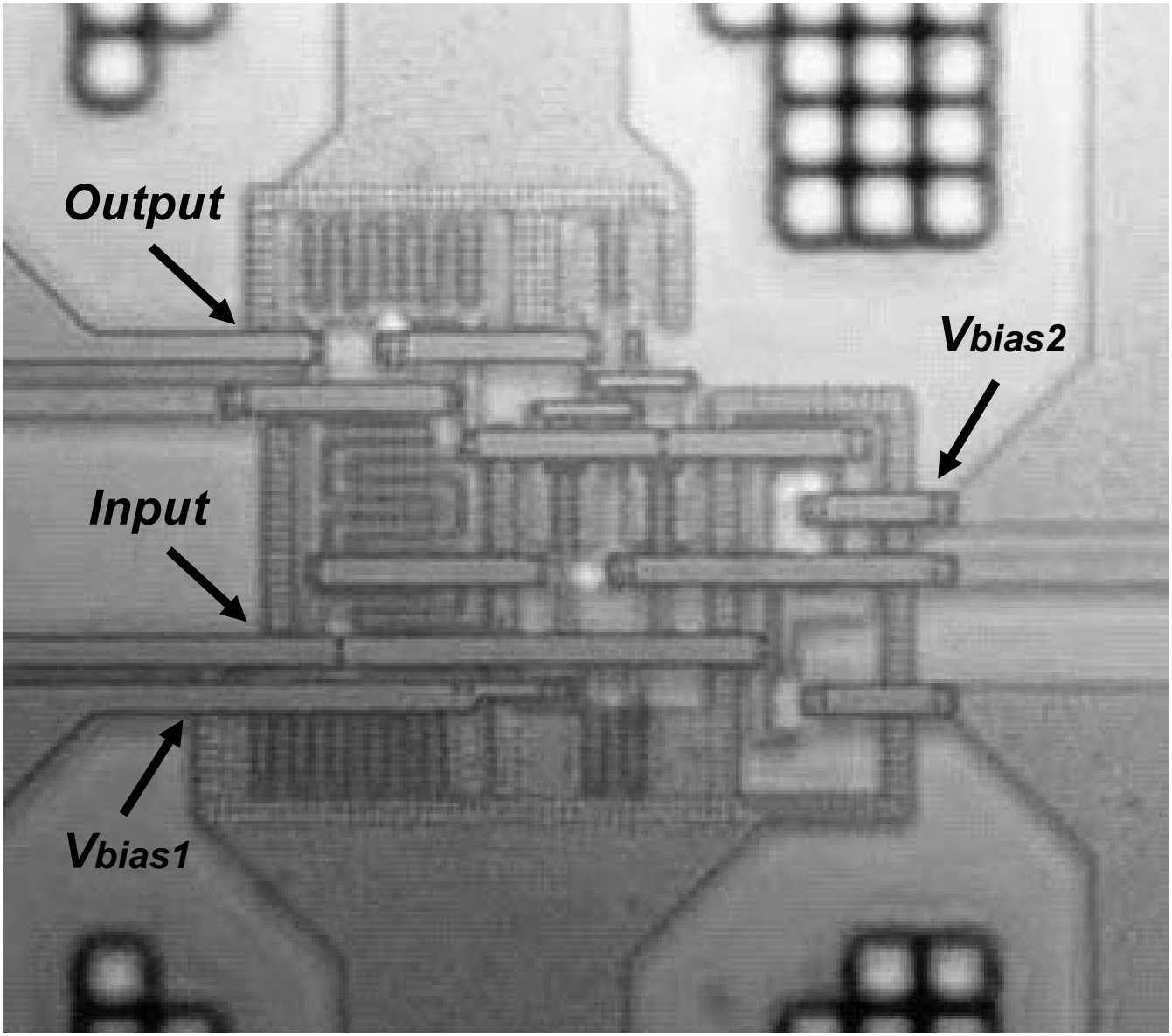


**Figure 17.7.5: Photo of the sustaining transresistance amplifier fabricated in TSMC's 0.35μm CMOS process.**


0-7803-8267-6/04 

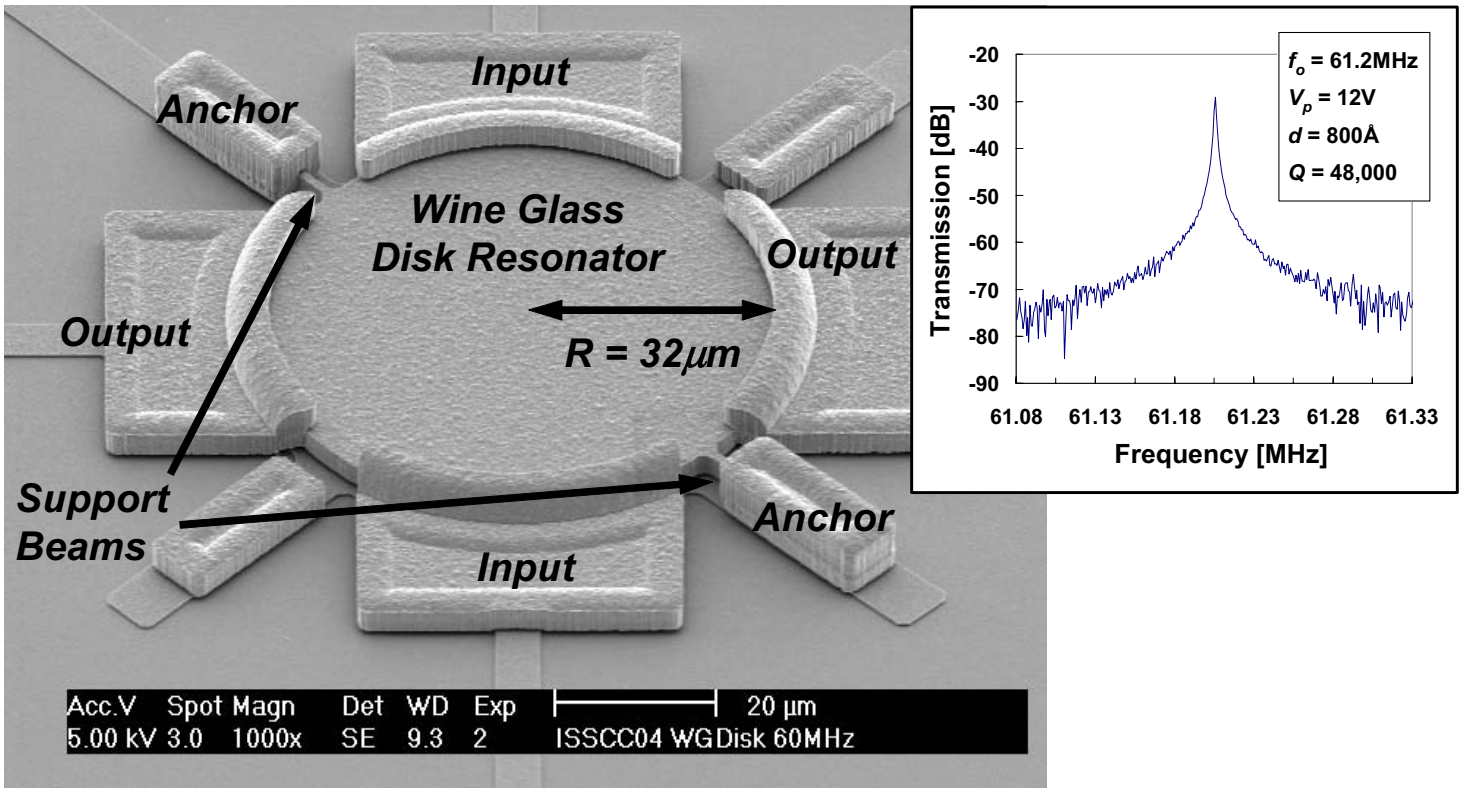


**Figure 17.7.6: Scanning electron micrograph (SEM) of a fabricated wine glass disk resonator with two supports, with its measured frequency characteristic.**

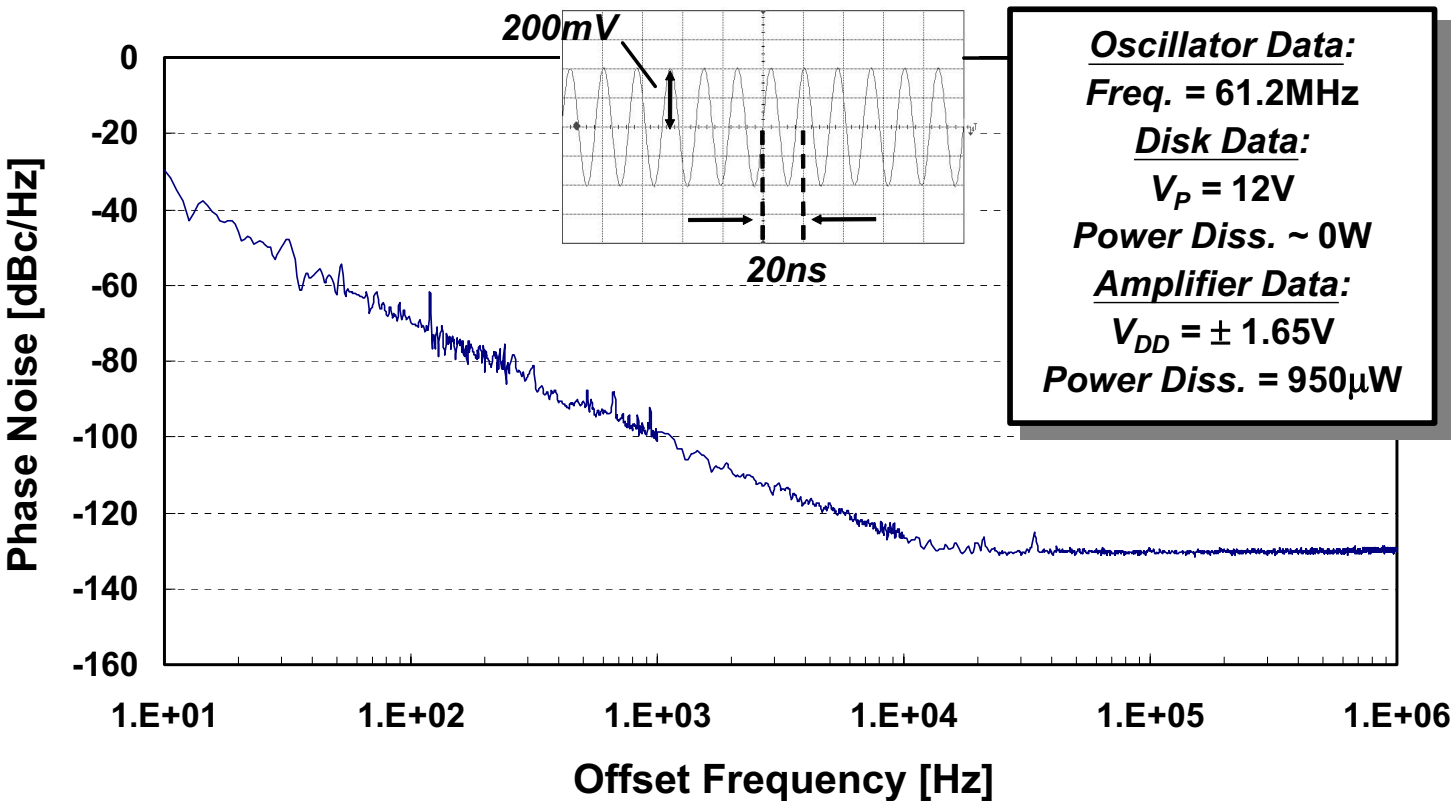


**Figure 17.7.7: Phase noise density versus carrier offset frequency plot for the micromechanical resonator oscillator of Figure 17.7.4, measured by an HP E5500 Phase Noise Measurement System.**


0-7803-8267-6/04 